Neutron-diffraction study of the magnetic and orbital ordering in 154SmNiO3 and 153EuNiO3

J. Rodriguez-Carvajal, S. Rosenkranz, M. Medarde, P. Lacorre, M. T Fernandez-Diaz, F. Fauth, V. Trounov

Neutron-diffraction study of the magnetic and orbital ordering in $^{154}SmNiO_3$ and $^{153}EuNiO_3$

J. Rodríguez-Carvajal*
Laboratoire Léon Brillouin (CEA-CNRS), Centre d'Etudes de Saclay, F-91191 Gif-sur-Yvette Cedex, France

S. Rosenkranz and M. Medarde
Labor für Neutronenstreuung ETHZ and PSI, CH-5232 Villigen PSI, Switzerland

P. Lacorre
Laboratoire des Fluorures, UPRES-A CNRS 6010, Université du Maine, F-72085 Le Mans Cedex 9, France

M. T. Fernandez-Díaz and F. Fauth
Institut Laue-Langevin, B.P. 156, 38042 Grenoble Cedex 9, France

V. Trounov
Petersburg Nuclear Physics Institute, 188358 Gatchina, Russia
(Received 16 July 1997)

Neutron-powder-diffraction experiments on $^{154}SmNiO_3$ and $^{153}EuNiO_3$ at different temperatures have been performed. At variance with the case of Pr and Nd nickelates, the metal-insulator transition temperature in these compounds are different from the Néel temperature ($T_{M\text{-}I}\approx 400$ K, $T_N\approx 230$ K for Sm and $T_{M\text{-}I}\approx 480$ K, $T_N\approx 220$ K for Eu) so that the magnetic ordering develops upon cooling in an insulating matrix. With decreasing temperature the crystal structure undergoes a 0.15% lattice expansion at $T_{M\text{-}I}$. The crystal symmetry $Pbnm$ does not change within the experimental error, but the Ni-O average distance increases and the superexchange angle Ni-O-Ni decreases slightly in the insulating regime. The magnetic structure of both compounds has the same propagation vector $\mathbf{k}=(\frac{1}{2},0,\frac{1}{2})$ as observed in Pr and Nd nickelates. This feature leads us to speculate that the orbital ordering responsible for the magnetic structure is a characteristic of the insulating state of the $RNiO_3$ series (at least for light rare earths R). A search for small nuclear superstructure peaks characterizing the orbital ordering has been carried out without success. The consequences of our experimental results are discussed in the context of current ideas about superexchange in oxides. [S0163-1829(98)01401-5]

I. INTRODUCTION

Perovskite oxides are currently of high interest because of the panoply of exotic physical properties they display. After the discovery of superconductivity in perovskite-related oxides, the colossal magnetoresistance observed in Mn-based perovskites is attracting the interest of condensed matter scientists.[1] Among the phenomena observed in these materials are different electronic processes like structural transitions induced by an external magnetic field, charge ordering, and orbital ordering due to cooperative Jahn-Teller (JT) effect.[2] Charge and orbital ordering in manganites are fascinating phenomena that deserve deeper studies using different experimental techniques, in order to determine precisely the real physics behind these concepts. These interesting physical properties of Mn perovskites appear on doping with holes (by substitution of an alkaline earth for the rare earth). Qualitatively, many properties of these materials can be understood within the classical scheme of a hole-doped Mott-Hubbard insulator in which double exchange, Hund coupling, and the Jahn-Teller effect play crucial roles. However a proper formulation of the theory is still lacking.

Rare-earth/nickel perovskites have some common characteristics to their Mn homologues but, concerning the electronic structure, they are placed at the boundary separating ''low-Δ metals'' and ''charge-transfer insulator.''[3] In nickelates $RNiO_3$ (R: rare earth) a metal-insulator (M-I) transition takes place as a function of temperature[4] but, in contrast to the manganites, no doping is needed to induce such a phenomenon. The transition temperature $T_{M\text{-}I}$ can be easily tuned by varying the rare earth. This temperature seems directly related to the steric effect induced by the R^{3+} cation, via the change of the superexchange angle Ni-O-Ni and hence the bandwidth.[5–7] The structural features accompanying the M-I transition for $R=$Pr and Nd, have been discussed extensively in Ref. 6, and can be summarized as follows: the cell volume increases on going from the metallic to the insulating regime as a consequence of a slight increase of the Ni-O distances ($\Delta d_{\text{Ni-O}}\approx +0.004$ Å). The increment of the Ni-O distances induces additional tilts of the NiO_6 octahedra that produce a diminution of the superexchange Ni-O-Ni angle ($\Delta\Theta_{\text{O-Ni-O}}\approx -0.5°$). At variance with $LaMnO_3$, no orbital ordering is apparent from the anisotropy of the Ni-O distances in NiO_6 octahedra, even if low spin $Ni^{3+}(t_{2g}{}^6e_g^1)$ is susceptible to the JT effect as is $Mn^{3+}(t_{2g}{}^3e_g^1)$. This is probably a manifestation of the more covalent character of the Ni oxides: the higher crystal field

in the latter makes the ionic picture less adequate than in Mn oxides. However, the magnetic structure observed for Pr and Nd compounds led us to postulate the existence of some kind of orbital ordering in these perovskites,[8] even if the structural distortion associated with this ordering is not detected by our experimental methods. In these two compounds the M-I transition temperature is also the Néel temperature. Both compounds become magnetically ordered in the insulating regime. This feature led some of us to think about an abnormal situation in which a spin-density-wavelike state existed in the vicinity of $T_{M\text{-}I}$ in the metallic state that condensed into the peculiar magnetic structure observed for Pr and Nd compounds in the insulating regime. The Sm and Eu compounds, in which both temperatures, T_N and $T_{M\text{-}I}$, are well separated, were good candidates to investigate the stability of this magnetic structure against the proximity of the metallic state. The high absorption of neutrons by natural Sm and Eu precluded a neutron experiment. The availability of ^{154}Sm and ^{153}Eu allowed us to perform a series of neutron experiments in order to complete the structural study performed with x-ray diffraction and to investigate the magnetic structure of these two members of the series.

II. EXPERIMENTAL AND DATA ANALYSIS

Powder samples of Sm and Eu nickelates were prepared starting from isotopic 99% enriched $^{154}Sm_2O_3$ and $^{153}Eu_2O_3$, respectively. We used the procedure described in Ref. 4. Several powder diffractometers at the Laboratoire Léon Brillouin (LLB) in Saclay and the Institute Laue-Langevin (ILL) in Grenoble, were used in this study. The banana-type diffractometer G4.1 ($\lambda \approx 2.43$ Å, graphite focusing monochromator, $2\theta_M \approx 42°$), was used for determining the magnetic structure and the evolution of the unit-cell parameters between 1.5 and 230 K. Several neutron-powder-diffraction patterns were collected by using a standard Orange cryostat (temperature stability better than 0.1 K). To investigate the structural changes across the M-I transition in the Sm case ($T_{M\text{-}I} \approx 400$ K) two high-resolution diffraction patterns were recorded at 375 and 410 K on the diffractometer 3T2 [Ge(335) at a takeoff angle of 90°, $\lambda = 1.22$ Å, $Q_{\max} = 9.2$ Å^{-1}). A furnace, with the sample under vacuum, was used to change the temperature of the sample above room temperature. The magnetic and crystal structures of the Eu compound were studied, between 1.5 and 200 K, using data collected on the ILL diffractometer D1A [Ge(115) at a takeoff angle of 120°, $\lambda = 1.91$ Å, and Ge(113) $\lambda = 2.99$ Å]. The absorption cross section of ^{153}Eu is still quite high but good quality diffraction patterns could be obtained by using a hollow vanadium sample can of diameters $\varnothing_{\text{internal}} = 9$ mm, and $\varnothing_{\text{external}} = 10$ mm. The diffractometer D1B of the ILL ($\lambda = 2.52$ Å), similar to G4.1 but with more flux, was used for a high counting experiment devoted to determining the presence and/or absence of superstructure peaks associated to the orbital ordering in $SmNiO_3$. The counting time for each of the two recorded patterns (420 and 320 K) was 36 h.

All data were analyzed using the Rietveld method for crystal and magnetic structure refinement with the program FULLPROF.[9] The peak shape in profile refinements was described by a pseudo-Voigt function. The parameters modeling the full width at half maximum of Bragg peaks (U, V, W in the Caglioti's formula) were refined close to the resolution function of the respective diffractometers, indicating very good sample quality. The background was either interpolated between a set of manually determined points or refined using a six-parameter polynomial function. The Fermi lengths of the different nuclear species were taken from Ref. 10. The magnetic form factor for Ni atoms was taken using the coefficients given in the International Tables[11] for the spin only, $\langle j_0 \rangle$, part of the Ni^{3+} free ion. For that of Sm^{3+} we used the dipolar approximation[12] and the coefficients given for $\langle j_0 \rangle$ and $\langle j_2 \rangle$ in Ref. 11. No evidence of magnetic ordering of the Eu^{3+} ions was found.

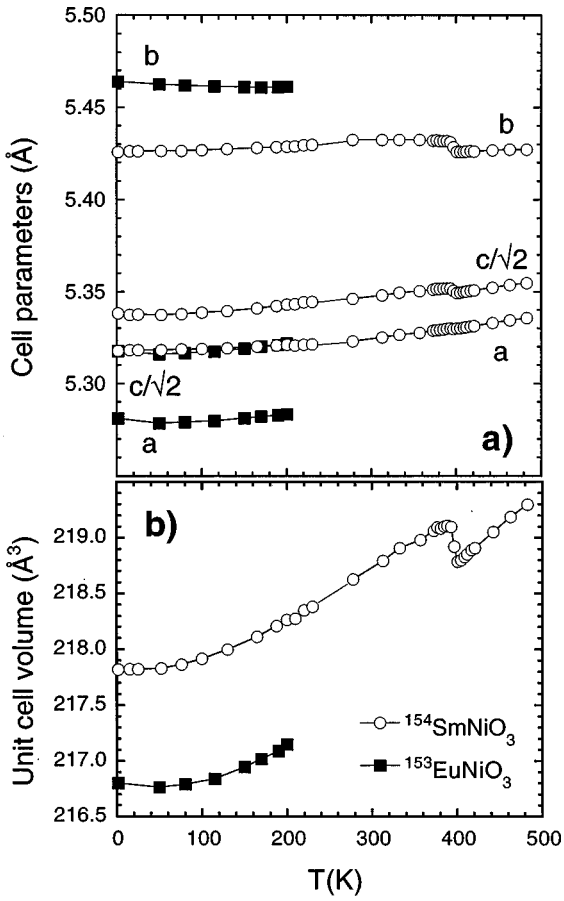

FIG. 1. (a) Cell parameters a, b, and $c/\sqrt{2}$ and (b) unit-cell volume of $^{154}SmNiO_3$ and $^{153}EuNiO_3$ as a function of temperature. Experimental points from different instruments have been grouped after wavelength correction as explained in the text.

The cell parameters obtained with different instruments were recalibrated by refining the neutron wavelength and zero point of the corresponding diffractometer in order to match the cell parameters obtained with x-ray diffraction at high temperature. After the correction of the wavelengths new full refinements of the diffraction patterns were performed.

III. RESULTS

A. Structural behavior

The temperature dependence of the cell parameters is displayed in Fig. 1. It is worth mentioning that $c/\sqrt{2}$ lies between a and b. This is the usual situation in perovskites

TABLE I. Structural parameters and conventional reliability indices obtained from the Rietveld refinement of the diffraction patterns of $^{154}SmNiO_3$ at both sides of the M-I transition and for $^{153}EuNiO_3$ at 1.5 K.

	$^{154}SmNiO_3$	$^{154}SmNiO_3$	$^{153}EuNiO_3$
Temperature	375 K	410 K	1.5 K
Space group	*Pbnm*	*Pbnm*	*Pbnm*
Rare earth ($4c$)			
($xy\frac{1}{4}$)			
x	0.9908(5)	0.9908(5)	0.9864(4)
y	0.0504(2)	0.0492(2)	0.0584(3)
B (Å^2)	0.70(3)	0.76(3)	0.10
Ni ($4b$)			
($\frac{1}{2}00$)			
B (Å^2)	0.36(2)	0.38(2)	0.32
O1 ($4c$)			
($xy\frac{1}{4}$)			
x	0.0808(6)	0.0799(5)	0.0861(5)
y	0.4855(5)	0.4862(5)	0.4796(5)
B (Å^2)	0.70(5)	0.70(4)	0.46
O2 ($8d$)			
(xyz)			
x	0.7076(4)	0.7080(4)	0.7022(4)
y	0.2929(3)	0.2933(3)	0.2961(4)
z	0.0426(3)	0.0413(3)	0.0434(3)
B (Å^2)	0.75(3)	0.65(3)	0.59
a (Å)	5.3301(1)	5.3316(1)	5.2811(1)
b (Å)	5.4296(1)	5.4242(1)	5.4641(1)
c (Å)	7.5680(2)	7.5661(2)	7.5110(2)
R_{wp} (%)	6.50	6.16	4.95
$R_{\rm exp}$ (%)	5.17	5.22	2.53
χ^2	1.58	1.39	3.83
R_B (%)	5.77	4.51	5.36

TABLE II. Interatomic distances (in Å) and angles (in degrees) calculated with the parameters given in the previous table. The distortion parameter Δ of a coordination polyhedron BO_N with an average B-O distance $\langle d\rangle$, is defined as $\Delta=(1/N)\Sigma_{n=1,N}\{(d_n-\langle d\rangle)/\langle d\rangle\}^2$. $\langle\omega\rangle$ is the average tilt angle of NiO_6 octahedra.

	$^{154}SmNiO_3$	$^{154}SmNiO_3$	$^{153}EuNiO_3$
Temperature	375 K	410 K	1.5 K
Space group	*Pbnm*	*Pbnm*	*Pbnm*
$d_{\rm Ni\text{-}O1}$ ($\times2$)	1.942(1)	1.940(1)	1.937(1)
$d_{\rm Ni\text{-}O2}$ ($\times2$)	1.961(2)	1.964(2)	1.966(2)
($\times2$)	1.953(2)	1.944(2)	1.955(2)
$\langle d_{\rm Ni\text{-}O}\rangle$	1.952(1)	1.949(1)	1.953(1)
Δ ($\times10^{-4}$)	0.16	0.29	0.36
Ni-O1-Ni ($\times2$)	154.0(1)	154.2(1)	152.0(1)
Ni-O2-Ni ($\times4$)	152.8(3)	153.4(3)	151.4(2)
$\langle$Ni-O-Ni$\rangle$	153.2(2)	153.7(2)	151.6(1)
$\langle\omega\rangle$	13.4(1)	13.2(1)	14.2(1)
$d_{R\text{-}O1}$	2.410(3)	2.418(3)	2.361(3)
$d_{R\text{-}O1}$	2.311(4)	2.314(4)	2.298(4)
$d_{R\text{-}O2}$ ($\times2$)	2.548(3)	2.554(3)	2.520(3)
$d_{R\text{-}O2}$ ($\times2$)	2.351(3)	2.355(2)	2.337(2)
$d_{R\text{-}O2}$ ($\times2$)	2.636(3)	2.632(2)	2.608(2)
$\langle d_{R\text{-}O}\rangle$	2.474(1)	2.477(1)	2.448(1)
Δ ($\times10^{-4}$)	25.47	24.40	24.30

where the primary distorting effect is steric. This is in contrast with $LaMnO_3$ in which the strong cooperative JT effect induces an orbital ordering distorting the MnO octahedra and gives rise to the so-called O' structure with $c/\sqrt{2}\leqslant a\leqslant b$. The neutron-diffraction experiments confirm the thermal expansion already determined with x-ray diffraction.[6]

The structural behavior observed across the M-I transition is similar to that observed for Pr and Nd compounds. In Tables I and II we have gathered the whole set of crystallographic parameters and geometrical data characterizing the crystalline structure of $SmNiO_3$ at both sides of the M-I transition. Crystallographic parameters of $EuNiO_3$ at low temperature have also been included. A plot of the observed and calculated powder-diffraction patterns of $^{154}SmNiO_3$ recorded on 3T2 just above the M-I transition is presented in Fig. 2(a). The low-temperature refined pattern of $EuNiO_3$ is depicted in Fig. 2(b).

The geometrical parameters relevant to the M-I transition are the average Ni-O distance and the superexchange angle. The later governs the transfer integral T_{dpd} determining the bandwidth and hence $T_{M\text{-}I}$. We have represented the behavior of these two geometrical parameters for five R cations in Fig. 3 as a function of temperature. We have used previously published data and our present results for $SmNiO_3$ and $EuNiO_3$ (see caption of Fig. 3). It is worth remarking that the average Ni-O distance in the insulating compounds is centered about 1.945 Å at low temperature, significantly higher than that (1.933 Å) corresponding to metallic $LaNiO_3$. The smooth increase of the average Ni-O distance, $\langle d(\text{Ni-O})\rangle$, with decreasing size of the rare-earth ions just reflects the evolution of the electronegativity along the $4f$ series (from 1.10 for La to 1.17 for Sm).[13] This is not the case for the average Ni-O-Ni angle, $\langle$Ni-O-Ni$\rangle$, which is, as expected, strongly dependent on the rare-earth size [see Fig. 3(b)].

B. Magnetic ordering

The neutron-powder-diffraction patterns of $SmNiO_3$ obtained below the Néel temperature ($T_N\approx230$ K) show the presence of small magnetic reflections that can be indexed by using the propagation vector $\mathbf{k}=(\frac{1}{2},0,\frac{1}{2})$. This is the same magnetic lattice as in Pr and Nd compounds, so the discussion we presented in Ref. 8 for determining the magnetic structure of the Pr and Nd compounds can be extended to the Sm case. Using the same magnetic model for Ni and Sm atoms as in the case of $NdNiO_3$, we have refined the neutron-diffraction patterns obtained on G4.1 from 1.5 up to 230 K. In Fig. 4(a) we show the observed and calculated diffraction patterns at 1.5 K. The magnetic structure is shown in Fig. 4(b).

As in the case of $NdNiO_3$, only half of the (001) planes of Sm^{3+} have a nonvanishing magnetic moment at Sm sites. This is the result of the cancellation of the molecular field at some R sites due to the particular spin arrangement of Ni ions. In the present case the weakness of the magnetic reflections makes the distinction between the equal-moment ar-

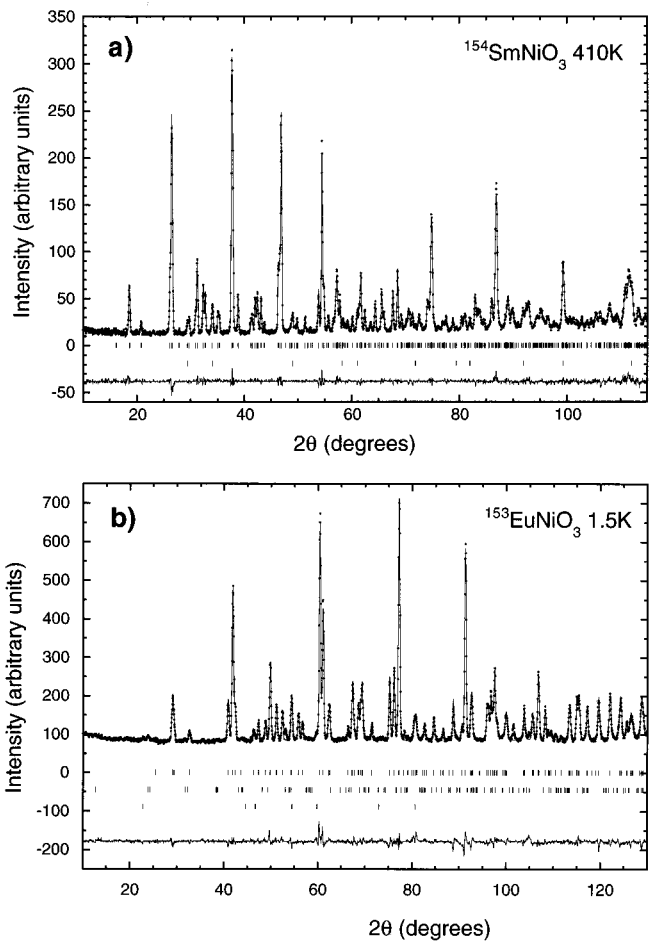

FIG. 2. (a) Observed (open circles), calculated, and difference (continuous lines) neutron-powder-diffraction patterns of $^{154}SmNiO_3$ at 410 K (metallic state) obtained in the diffractometer 3*T*2. The second row of reflection markers represent the contribution of a minor NiO impurity. (b) Observed and calculated powder-diffraction patterns of $^{153}EuNiO_3$ at 1.5 K obtained in the diffractometer D1A.

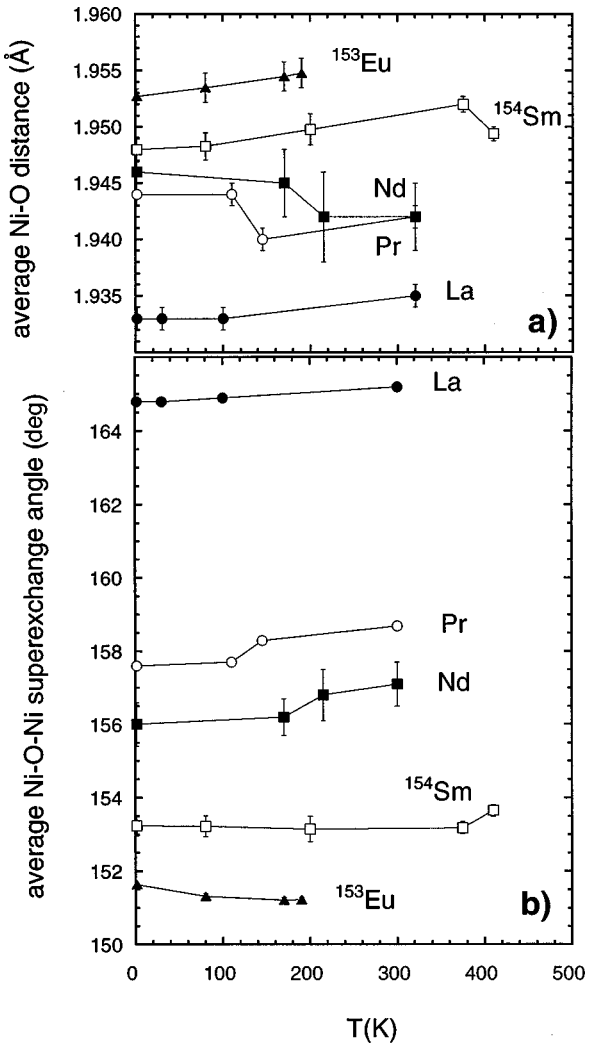

FIG. 3. (a) Average Ni-O distances and (b) average superexchange angle Ni-O-Ni, vs temperature for different RNiO$_3$ compounds R=La, Pr, Nd (Ref. 6), ^{154}Sm, and ^{153}Eu (this work), determined from neutron-powder-diffraction refinements.

rangement for Sm and the model we are discussing quite difficult. Nevertheless the presence of the same propagation vector as in the Nd compound, suggests the same behavior.

In Fig. 5, the value of the Ni magnetic moment in $SmNiO_3$ has been represented as a function of temperature. The continuous curve has been calculated by using the Brillouin function with a saturation moment $\mu_{sat}=0.85\ \mu_B$ and a transition temperature $T_N=230$ K.

The refinement of the crystal and magnetic structure of $EuNiO_3$ [see Fig. 2(b)] was affected by a relatively large absorption, so the accuracy of the refined parameters is not as good as in the Sm case. The magnetic structure of $EuNiO_3$ produces Bragg peaks indexed with the propagation vector $\mathbf{k}=(\frac{1}{2},0,\frac{1}{2})$ and is the same as in the other compounds. The temperature behavior of the Ni moment is also displayed in Fig. 5 together with the calculated moment from the Brillouin function with $\mu_{sat}=1.18\ \mu_B$ and $T_N=220$ K. No ordered magnetic moment has been detected in the Eu^{3+} ions, however the weakness of the magnetic reflections does not allow us to discard this possibility. To be noticed is the difference between the saturation value of the Ni magnetic moment in $PrNiO_3$ ($\approx 0.9\ \mu_B$), $NdNiO_3$ ($\approx 0.9\ \mu_B$), and $SmNiO_3$ ($\approx 0.9\ \mu_B$) and $EuNiO_3$ ($\approx 1.2\ \mu_B$). The anomalous large value found in the Eu compound probably arises from the difficulties in properly handling the absorption correction in the treatment of the diffraction patterns in the presence of weak magnetic reflections. The absorption normally affects the scale factor and the thermal parameters. The atomic coordinates are, however, almost independent of the absorption coefficient used in the refinement. Nevertheless, the increase of the magnetic moment of Ni in the Eu compound could have a real physical significance, in the sense that if the covalence of the Ni-O bonding increases on going to smaller R, the partial electron transfer from oxygen to Ni increases the effective moment at Ni sites. This point needs confirmation on a sample of RNiO$_3$ with a smaller rare earth.

IV. DISCUSSION

The ground-state magnetic ordering of $SmNiO_3$ and $EuNiO_3$ is of the same type as that already observed for Pr and Nd nickelates, so it seems that the exchange interactions

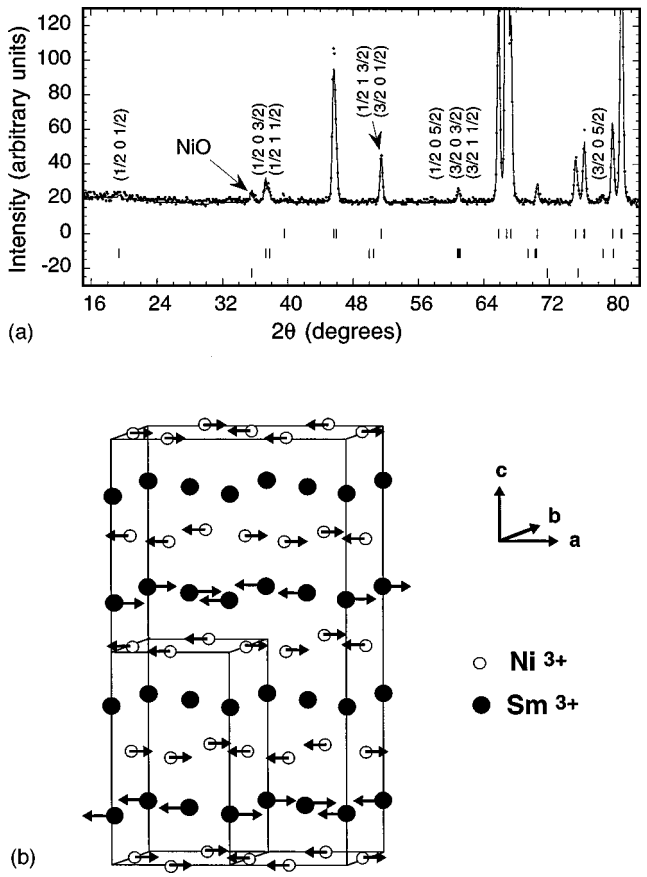

FIG. 4. (a) Observed (open circles), calculated, and difference (continuous lines) neutron-powder-diffraction patterns of $^{154}SmNiO_3$ at 1.5 K (insulating state) obtained in the diffractometer G4.1. The magnetic reflections are explicitly indexed. (b) Magnetic structure of $^{154}SmNiO_3$. In $^{153}EuNiO_3$ the arrangement of the Ni moments is identical, however no ordering of the Eu sublattice has been observed.

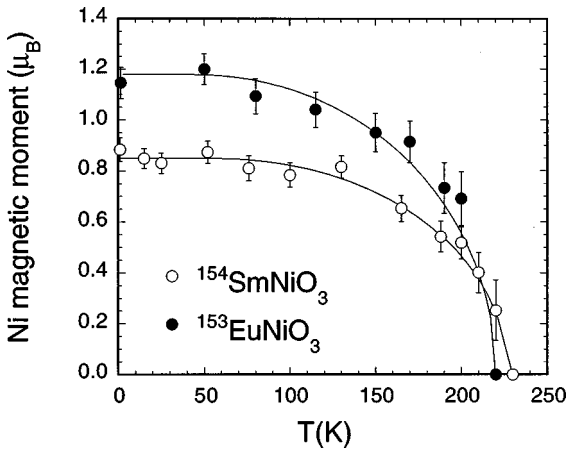

FIG. 5. Staggered Ni magnetic moment (in Bohr magnetons) as a function of temperature of $^{154}SmNiO_3$ and $^{153}EuNiO_3$. The continuous lines correspond to the calculations using the Brillouin function.

coupling nearest Ni neighbors in the insulating state have alternating opposite signs. This is a strong conclusion that can be obtained from a straightforward analysis of a classical Heisenberg Hamiltonian (see Appendix). Thus, within the widely accepted framework of the Goodenough-Kanamori rules[14,15] for the sign of the exchange interactions in insulators, the observed magnetic structure could only be the result of an orbital ordering allowing the alternation of positive and negative exchange interactions. In Fig. 6(a) is shown the orbital ordering existing in $LaMnO_3$ (Ref. 16) and, in Fig. 6(b) and Fig. 6(c), the two possible orbital orderings for $RNiO_3$ (R=Pr, Nd, Sm, Eu) are depicted. In the case of $LaMnO_3$ the orbital ordering does not break down the crystallographic symmetry of the orbital-disordered phase ($Pbnm$) existing above the Jahn-Teller transition temperature $T_{JT}\approx 790$ K. The orbital ordering is experimentally detected just by a change in the local geometry of MnO_6 octahedra.[17] In $RNiO_3$ the orbital ordering compatible with the magnetic structure should make Ni atoms nonequivalent, so a change of crystallographic symmetry is expected. A group theory analysis of the space groups compatible with a structural phase transition characterized by a propagation vector $q=(\frac{1}{2},0,\frac{1}{2})$, identical to that of the magnetic structure in the setting $Pbnm$, leads to crystal structures belonging to two different settings of the space groups $Bb2_1m$ ($\mathbf{a}'=2\mathbf{a}$, $\mathbf{b}'=\mathbf{b}$, $\mathbf{c}'=2\mathbf{c}$), $P2_1$ ($\mathbf{a}'=\mathbf{a}+\mathbf{b}$, $\mathbf{b}'=\mathbf{b}$, $\mathbf{c}'=\mathbf{a}-\mathbf{c}$) or $P2_1/c$ ($\mathbf{a}'=\mathbf{a}+\mathbf{b}$, $\mathbf{b}'=\mathbf{b}$, $\mathbf{c}'=\mathbf{a}-\mathbf{c}$), (see Ref. 18). The latter cannot describe an orbital ordering compatible with the observed magnetic structure, but the former is the most symmetric group satisfying this prescription. In Table III we have written the atom positions of $RNiO_3$ in the $Bb2_1m$ setting. The two orbital orderings shown in Fig. 6 have $Bb2_1m$ symmetry and are compatible with the observed magnetic structure and the Goodenough-Kanamori rules for superexchange (see Appendix).

If the orbital ordering produces a significant distortion of the NiO_6 octahedra, it could be possible to observe superstructure peaks corresponding to the propagation vector $\mathbf{q}=(\frac{1}{2},0,\frac{1}{2})$ in the paramagnetic insulating state. We could not detect such a change in the crystal structure in our earlier work; thus we have attempted to detect the signature of the orbital ordering (that we assume to be established in the insulating regime) by a high intensity neutron-diffraction measurement. The comparison of diagrams at low (insulating state) and high (metallic state) temperature is shown in Fig. 7. We could not see any indication of superstructure peaks. We have made an estimation of the oxygen displacements, for the orbital ordering proposed in Fig. 6, with respect to the average cell in the $Pbnm$ setting that is compatible with the observed diffraction patterns. For that we performed a simulation of the observed diffraction pattern, considering that all the atoms, except the oxygen atoms deriving from O(2) in the basal plane, conserve the $Pbnm$ structure. We produced a synthetic diffraction pattern calculated with the orbital-disordered structure with a counting statistic similar to the real diffraction pattern obtained in D1B, but with a high Q range (as in 3T2). We started the refinement of the synthetic diffraction pattern using deformed NiO_6 octahedra. The re-

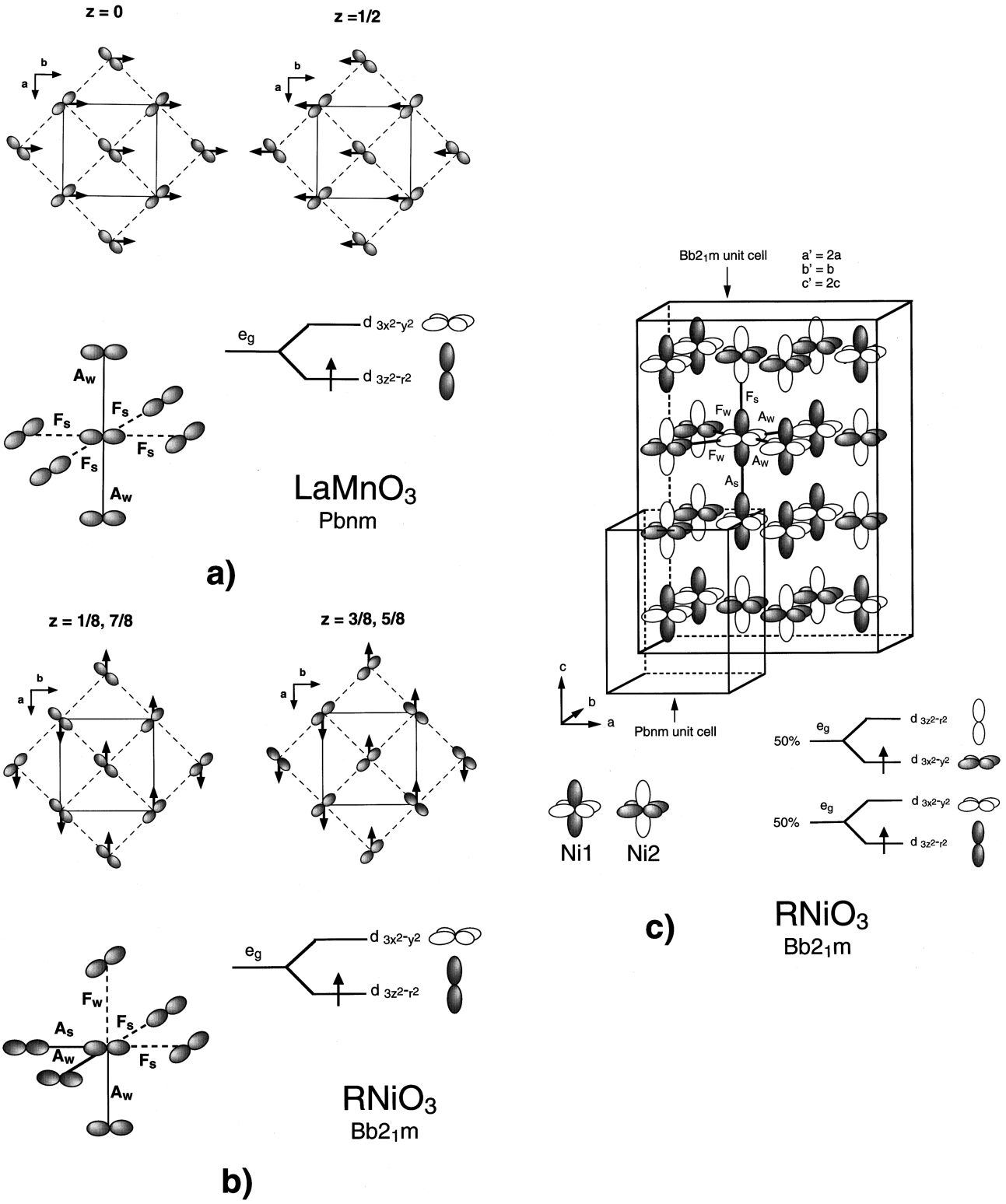

FIG. 6. (a) Schematic representation of the orbital ordering in $LaMnO_3$. (b) and (c) two possible orbital orderings in $RNiO_3$ (R = Pr,Nd,Sm) compatible with the $Bb2_1m$ symmetry. We have represented the occupied e_g orbital of LS-$Ni^{3+}(t_{2g}{}^6e_g{}^1)$ and $Mn^{3+}(t_{2g}{}^3e_g{}^1)$ by dark lobes that mimics the electron density. The relative orientation of the lobes give rise to roughly four types of exchange interactions A_W, A_S, F_W, and F_S. The projection of the unit cell is referred to the $Bb2_1m$ setting. See Appendix for details.

finement of the Ni-O distances (using generalized coordinates) was done in the $Bb2_1m$ setting, as given in Table III, but keeping the $Pbnm$ constraints, except for oxygen atoms O21, O22, O23, and O24. We arrived at a situation in which a significant distortion can exist but the superstructure peaks are too weak to be observed. An example of such a distortion is given by the oxygen, positions (in italics) in Table III. The most intense superstructure peak for that case is 2×10^{-4} times smaller than the most intense fundamental reflection, but the Ni-O distances are

TABLE III. Atom positions of the orbitally ordered $R\mathrm{NiO_3}$ compounds. The symmetry is $Bb2_1m$ (standard setting $Cmc2_1$) with two Wyckoff positions:

$$+(0,0,0);(\tfrac{1}{2},0,\tfrac{1}{2})$$

$(8b)$ 1 $(x,y,z);(-x,y+\tfrac{1}{2},z);(x,y,-z);(-x,y+\tfrac{1}{2},-z)$

$(4a)$ ..m $(x,y,0);(-x,y+\tfrac{1}{2},0)$.

The particular values of the atom coordinates correspond to those of the super-group $Pbnm$ for $T=375$ K. Fractional coordinates are referred to the unit cell: $\mathbf{a}'=2\mathbf{a}$, $\mathbf{b}'=\mathbf{b}$, $\mathbf{c}'=2\mathbf{c}$. The origin of the new cell with respect to the $Pbnm$ cell is $(\tfrac{1}{4},0,\tfrac{1}{4})$. Coordinates in italics represents a distortion of the NiO_6 octahedra giving rise to small superstructure peaks that cannot be seen in our experimental conditions (see text for explanation).

Atom	$Bb2_1m$ site	x	y	z	$Pbnm$ site
Sm1	$(4a)$	0.36983	0.05029	0	Sm $(4c)$
Sm2	$(4a)$	0.36983	0.05029	$\frac{1}{2}$	
Sm3	$(8b)$	0.11983	0.44971	0.25000	
Ni1	$(8b)$	0.12500	0.00000	0.12500	Ni $(4b)$
Ni2	$(8b)$	0.12500	0.00000	0.37500	
O11	$(4a)$	0.41497	0.48426	0	O1 $(4c)$
O12	$(4a)$	0.41497	0.48426	$\frac{1}{2}$	
O13	$(8b)$	0.16497	0.01574	0.25000	
O21	$(8b)$	0.22831	0.29248	0.39595	O2 $(8d)$
		0.22843	*0.29282*	*0.39595*	
O22	$(8b)$	0.22831	0.29248	0.89595	
		0.22700	*0.28899*	*0.89570*	
O23	$(8b)$	0.47831	0.20752	0.14595	
		0.47996	*0.20275*	*0.14623*	
O24	$(8b)$	0.47831	0.20752	0.35405	
		0.47778	*0.20881*	*0.35420*	

$$d(\text{Ni1-O})=\{2\times1.9413,1.9513,1.9346,1.9493,1.9616\}$$

$$\Rightarrow\text{Distortion:}\quad 0.2\times10^{-4},$$

$$d(\text{Ni2-O})=\{2\times1.9413,1.9607,1.9749,1.9913,1.9251\}$$

$$\Rightarrow\text{Distortion:}\quad 1.3\times10^{-4}.$$

This is an artificial case, but it illustrates the lack of sensitivity of the diffraction pattern to small distortions conserving the average Ni-O distances and the average tilt angle of octahedra for the present structure.

In the field of magnetic intermetallic compounds there are many cases in which spin arrangements of the type $(++--)$ along a crystallographic direction are observed.[19] In these systems the Ruderman-Kittel-Kasuya-Yosida (RKKY) interaction makes it possible to have second and further neighbor exchange integrals of the same order of magnitude as that for first neighbors, so that propagation vectors of the type $\mathbf{k}=\boldsymbol{\tau}/4$ ($\boldsymbol{\tau}$ is a reciprocal lattice vector) are stabilized in simple structures. It seems unlikely that interactions similar to RKKY type exist in insulators. The scheme of orbital ordering allows the explanation of the observed magnetic structure in terms of semiempirical rules that seem to work in many cases. However, the effective existence of the orbital ordering still remains to be demonstrated in $R\mathrm{NiO_3}$ compounds. The availability of single crystals and/or ''zero matrix'' isotopic mixtures of Sm and Ni ions, so that $b(\mathrm{Sm})\approx b(\mathrm{Ni})\approx0$, seems to be of absolute necessity to unambiguously state that orbital ordering is a relevant concept in these materials. The isotopic sample is being prepared for future experiments. Another possibility is that our ideas about superexchange interactions are too simplistic and the Goodenough-Kanamori rules do not apply to the present case. In any case, the existence of other subtle interactions able to stabilize the observed spin arrangement should not be disregarded.

ACKNOWLEDGMENT

We are indebted to the Russian Foundation of Fundamental Researches for making possible the development of this work.

APPENDIX

We demonstrate that a uniform (same sign) distribution of the exchange interactions between nearest neighbors in the perovskite Ni lattice is incompatible with the experimental results obtained for $R\mathrm{NiO_3}$. For simplicity we consider the simple cubic perovskite lattice. The orthorhombic nature of the compounds does not substantially change the conclusion. The experimental ground-state propagation vector with respect to the ''pseudocubic'' subcell is $\mathbf{k}=(\frac{1}{4},\frac{1}{4},\frac{1}{4})$. We consider that the magnetic ordering at $T=0$ corresponds to the minimum energy described by the classical Heisenberg energy:

$$E=-\sum J_{ij}\mathbf{S}_i\cdot\mathbf{S}_j, \tag{A1}$$

where $\mathbf{S}_i$ are considered as classical spins at site ''i'' interacting with the spin at site ''j'' through the exchange integral J_{ij}. Whereas there is no rigorous expression for J_{ij} in real insulating materials, we assume as valid the qualitative expressions for J given by Zeiger and Pratt[20] in their description of the semiempirical Goodenough-Kanamori rules. J depends on the transfer integral T, the electrostatic energy U and, eventually, on the intra-atomic exchange J^{intra}. The expression of J is formed by a set of contributions involving (a) both orbitals are half filled (AF): $J_{(1)}\sim-T_{dpd}^2/U$, (b) one orbital is half filled and the other is empty or full (F): $J_{(2)}\sim T_{dpd}^2J^{\mathrm{intra}}/U^2$, and (c) direct exchange J_{direct} (F) (see Ref. 20 for details). The most important term is generally $J_{(1)}$ but qualitative predictions of the relative strengths and signs can be made based on the geometrical characteristics of the cation-anion-cation bonds. The consideration of anisotropic exchange, single-ion anisotropy, dipolar, or higher-order (biquadratic for instance) spin interactions will not change our conclusions. This is so if we consider, as is the common belief in insulators, that the isotropic exchange, between the spins of two not too distant atoms, is the most important term responsible for the magnetic ordering. The Fourier transform of Eq. (A1) permits us to get a finite expression of the magnetic energy (if we consider that $J_{ij}=0$ for $R_{ij}>R_o$) as a function of the exchange parameters and

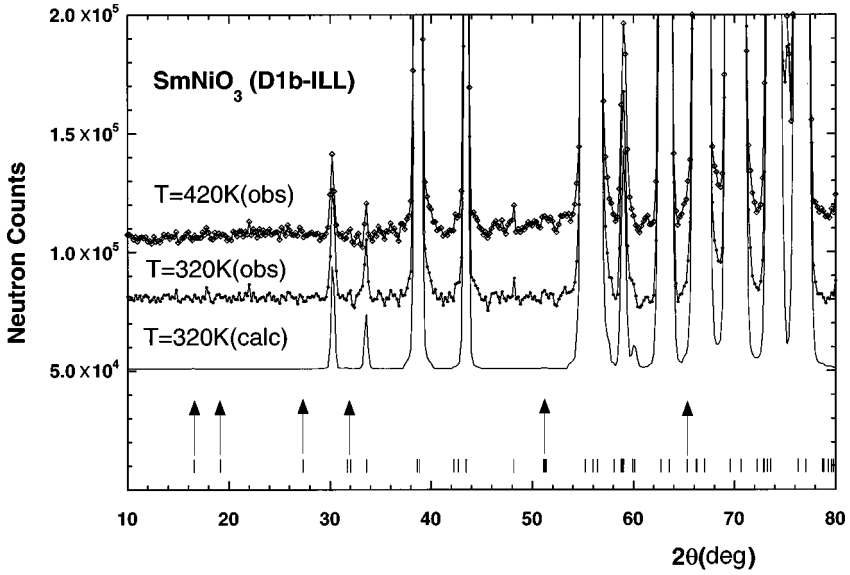

FIG. 7. Background corrected diffraction patterns obtained at 420 and at 320 K on D1B. No evidence of nuclear superstructure peaks coming from the orbital ordering is observed. The calculated pattern for the model given in Table III is also shown. Arrows indicate the positions at which nuclear $\mathbf{q}=(\frac{1}{2},0,\frac{1}{2})$ superstructure peaks, characterizing the orbital ordering, are expected to be more easily seen.

the propagation vector (see Ref. 21). For the perovskite lattice it can be written up to the fourth-nearest neighbors as

$$\begin{aligned} J(\mathbf{k}) = -E/NS^2 = {} & 2J_1\{\cos 2\pi k_x + \cos 2\pi k_y + \cos 2\pi k_z\} \\ & + 2J_2\{\cos 2\pi(k_x+k_y) + \cos 2\pi(k_x-k_y) + \cos 2\pi(k_x \\ & + k_z) + \cos 2\pi(k_x-k_z) + \cos 2\pi(k_y+k_z) + \cos 2\pi(k_y \\ & - k_z)\} + 2J_3\{\cos 2\pi(k_x+k_y+k_z) + \cos 2\pi(k_x-k_y \\ & + k_z) + \cos 2\pi(k_x-k_y-k_z) + \cos 2\pi(k_x+k_y-k_z)\} \\ & + 2J_4\{\cos 4\pi k_x + \cos 4\pi k_y + \cos 4\pi k_z\}, \end{aligned} \tag{A2}$$

where N is the number of magnetic ions and S is the spin value. The ground-state propagation vector is obtained by maximizing $J(\mathbf{k})$ with respect to $\mathbf{k}$. The above expressions for J lead clearly to $|J_1| \gg |J_i|$ $(i=2,3,4)$, so if we neglect next-nearest and farther neighbors interactions, $J(\mathbf{k})$ is maximum for $\mathbf{k}=(0,0,0)$ (ferromagnetism) if $J_1>0$ or for $\mathbf{k}=(\frac{1}{2},\frac{1}{2},\frac{1}{2})$ if $J_1<0$. The latter configuration corresponds to the G-type magnetic structure observed in the majority of perovskite oxides ABO_3 having a single type of B ion.

Considering propagation vectors of the form $\mathbf{k}=(k,k,k)$, the above expression simplifies to

$$\begin{aligned} J(k) = {} & 6J_2 + 6(J_1+J_3)\cos 2\pi k + 6(J_2+J_4)\cos 4\pi k \\ & + 2J_3 \cos 6\pi k. \end{aligned} \tag{A3}$$

It is straightforward to verify that $k=\frac{1}{4}$ could be a maximum of Eq. (A3) ($dJ(k)/dk=0$ and $d^2J(k)/dk^2<0$) only if $J_1=0$ and $J_2+J_4>0$. These conditions are necessary for $k=\frac{1}{4}$ to be the ground state but not sufficient. These conditions are contrary to what is expected from superexchange theory in insulators applied to the perovskite lattice, for which J_1 should be the most important term.

The effect of an orbital e_g ordering is to make J between nearest neighbors of different sign depending on whether neighboring cations have a half filled or empty orbital σ bond to the intervening anion. The case of $LaMnO_3$ is well known. The Jahn-Teller effect in this compound makes the nearest-neighbor interaction positive in the a-b plane and negative along c, so the exchange parameter J_1 is split as $J_{1x} \approx J_{1y} = J_1 \neq J_{1z} = J_1'$. The expression (A2) considering only next-nearest neighbors is written as

$$J(\mathbf{k}) = 2J_1\{\cos 2\pi k_x + \cos 2\pi k_y\} + 2J_1' \cos 2\pi k_z.$$

For $J_1>0$ and $J_1'<0$, $J(\mathbf{k})$ is maximum for $\mathbf{k}=(0,0,\frac{1}{2})$, that corresponds to the A-type magnetic structure observed for $LaMnO_3$.

In the case of $RNiO_3$ compounds the orbital ordering is peculiar. In their magnetic structure each Ni atom sees three Ni neighbors coupled ferromagnetically and three antiferromagnetically, so that $\mathrm{sign}[J(\mathbf{R}_i,\mathbf{R}_i+\mathbf{r}_\alpha)] = -\mathrm{sign}[J(\mathbf{R}_i,\mathbf{R}_i-\mathbf{r}_\alpha)]$, where $\mathbf{r}_\alpha$ is [100], [010], or [001]. Thus the common assumption of parity (each Ni atom is a center of symmetry of the spin Hamiltonian) for the exchange integral between an atom and the six nearest neighbors in the simple perovskite lattice is not fulfilled. Actually, the above conditions for nearest neighbors in the perovskite lattice suffice to stabilize the observed propagation vector. However, the simple analysis presented for a primitive cubic lattice is no longer possible because of the disappearance of the center of symmetry, which is a characteristic of atoms located in a Bravais lattice.

In previous work,[7,8] the proposed orbital ordering was not described in detail. The two degenerate e_g orbitals, $d_{x^2-y^2} = \sqrt{3}/2(x^2-y^2)$ and $d_{z^2} = d_{3z^2-r^2} = \frac{1}{2}(3z^2-r^2)$, split as

$$\psi_g = c_1 d_{x^2-y^2} + c_2 d_{3z^2-r^2},$$

$$\psi_e = c_2 d_{x^2-y^2} - c_1 d_{3z^2-r^2}.$$

Here x,y,z are local coordinates related to a particular NiO_6 octahedron. They can be oriented with respect to the crystallographic cell in different directions. The coefficients c_1 and c_2 can be different for the two types of Ni existing in the

cell. If the coefficients are the same for all the Ni ions in the cell, the orbitals can be distinguished by their orientation with respect to the crystallographic cell. In such a case if $c_2 > c_1$, as for $LaMnO_3$, the d_{z^2}-symmetry-type orbital is predominant. In Fig. 6(a) this type or orbital ordering is illustrated for $LaMnO_3$ and in Fig. 6(b) a $Bb2_1m$-symmetry-compatible d_{z^2}-orbital ordering for $R\mathrm{NiO}_3$ compounds in the insulating state. The other possible orbital ordering is illustrated in Fig. 6(c), it corresponds to a site (Ni1, for instance) in which $c_1 > c_2$ and to another site (Ni2) with $c_2 > c_1$. This $d_{x^2-y^2}/d_{z^2}$-orbital ordering was proposed for the first time in Ref. 8. The d_{z^2}-orbital ordering should produce a two long and four shorter Ni-O distances, whereas the $d_{x^2-y^2}/d_{z^2}$-orbital ordering should give a two short and four longer Ni-O distances. It is more probable that the actual orbital ordering in the $R\mathrm{NiO}_3$ compounds is of the $d_{x^2-y^2}/d_{z^2}$ type, because the expected distortion is smaller.

The orientation of the orbital lobes depicted in Fig. 6 gives rise to roughly four types of exchange interactions A_W, A_S, F_W, and F_S, verifying the following relations: $-J(A_S) > -J(A_W) \approx J(F_S) > J(F_W) \approx 0$. These interactions give the $\mathbf{k} = (\frac{1}{2}, 0, \frac{1}{2})$ magnetic ground state characterizing the $R\mathrm{NiO}_3$ perovskites in the insulating regime.

*Corresponding author. Electronic address: juan@bali.saclay.cea.fr

[1] R. von Helmolt *et al.*, Phys. Rev. Lett. **71**, 2331 (1993); Y. Tokura *et al.*, J. Phys. Soc. Jpn. **63**, 3931 (1994); S. Jin, M. McCormack, T. H. Tiefel, and R. Ramesh, J. Appl. Phys. **76**, 6929 (1994); R. von Helmolt *et al.*, J. Appl. Phys. **76**, 6925 (1994).

[2] Z. Jirák *et al.*, J. Magn. Magn. Mater. **53**, 153 (1985); A. Asamitsu *et al.*, Nature (London) **373**, 407 (1995); Y. Tomioka *et al.*, Phys. Rev. Lett. **74**, 5108 (1995).

[3] J. Zaanen, G. A. Sawatzky, and J. W. Allen, Phys. Rev. Lett. **55**, 418 (1985); J. B. Torrance, P. Lacorre, G. Asavaroengchai, and R. Metzger, J. Solid State Chem. **90**, 168 (1991); Physica C **182**, 351 (1991).

[4] P. Lacorre, J. B. Torrance, J. Pannetier, A. I. Nazzal, P. W. Wang, and T. C. Huang, J. Solid State Chem. **91**, 225 (1991).

[5] J. B. Torrance, P. Lacorre, A. I. Nazzal, E. J. Ansaldo, and C. Niedermayer, Phys. Rev. B **45**, 8209 (1992).

[6] J. L. García-Muñoz, J. Rodríguez-Carvajal, P. Lacorre, and J. B. Torrance, Phys. Rev. B **46**, 4414 (1992).

[7] M. Medarde, J. Phys.: Condens. Matter **9**, 1679 (1997).

[8] J. L. García-Muñoz, J. Rodríguez-Carvajal, and P. Lacorre, Europhys. Lett. **20**, 241 (1992); J. L. García-Muñoz, J. Rodríguez-Carvajal, and P. Lacorre, Phys. Rev. B **50**, 978 (1994).

[9] J. Rodríguez-Carvajal, Physica B **192**, 55 (1993).

[10] V. F. Sears, Neutron News **3**, 26 (1992).

[11] *International Tables for Crystallography*, edited by A. J. C. Wilson (Kluwer-Academic, London, 1992), Vol. C, p. 391.

[12] See, for instance, S. W. Lovesey, *Theory of Neutron Scattering from Condensed Matter* (Clarendon, Oxford, 1986), Vol. 2, p. 6.

[13] J. Emsley, *The Elements*, 3rd ed. (Oxford University Press, Oxford, 1996).

[14] J. B. Goodenough, Phys. Rev. **100(2)**, 564 (1955).

[15] J. Kanamori, J. Phys. Chem. Solids **10**, 87 (1959).

[16] E. O. Wollan and W. C. Koehler, Phys. Rev. **100**, 545 (1955); W. C. Koehler and E. O. Wollan, J. Phys. Chem. Solids **2**, 100 (1957).

[17] J. Rodríguez-Carvajal, M. Hennion, F. Moussa, L. Pinsard, and A. Revcolevschi, Physica B **234-236**, 848 (1997).

[18] H. T. Stokes and D. M. Hatch, *Isotropy Subgroups of the 230 Crystallographic Space Groups* (World Scientific, Singapore, 1988).

[19] J. Rossat-Mignod, in *Methods of Experimental Physics*, edited by K. Sköld and D. L. Price (Academic, Orlando, 1987), Vol. 23, Pt. C, pp. 59–167.

[20] H. J. Zeiger and G. W. Pratt, *Magnetic Interactions in Solids* (Clarendon, Oxford, 1973).

[21] D. H. Lyons and T. A. Kaplan, Phys. Rev. **120**, 1580 (1960); see also M. J. Freiser, Phys. Rev. **123**, 2003 (1961).